Assessment of Flow Characteristics at Two Locations in an Energetic Tidal Channel

Assessment of Flow Characteristics at Two Locations in an Energetic Tidal Channel

Torrens-Spence, H., Schmitt, P., Frost, C., Benson, I., MacKinnon, P., & Whittaker, T. (2017). Assessment of Flow Characteristics at Two Locations in an Energetic Tidal Channel. Paper presented at European Wave and Tidal Energy Conference, Cork, Ireland.

Assessment of Flow Characteristics at Two Locations in an Energetic Tidal Channel

Hanna Torrens-Spence[#1], Pál Schmitt[#2], Carwyn Frost[#3], Ian Benson[#4], Pauline Mackinnon[#5], Trevor Whittaker[#6]

[#]*School of Natural and Built Environment, Queen's University Belfast*
David Keir Building, Belfast, Northern Ireland

[1]htorrensspence01@qub.ac.uk

[2]p.schmitt@qub.ac.uk

[3]c.frost@qub.ac.uk

[4]ian.benson@qub.ac.uk

[5]p.mackinnon@qub.ac.uk

[6]t.whittaker@qub.ac.uk

***Abstract*—Inflow turbulence can impact a turbine's power performance and load conditions and also affects wake recovery. At array scale, changes in flow conditions across a site impact the energy yield, performance and load conditions of turbines. Understanding the variation of flow conditions in time and space at deployment sites is therefore important to the tidal stream energy industry.**

Tidal flow field data of sufficient detail to allow turbulence characterisation remains relatively scarce. Traditional three or four beam Acoustic Doppler Current Profilers (ADCPs), which are commonly used for tidal flow resource characterisation, are limited by their spatial and temporal resolution and by the assumption of flow homogeneity across their beams. Higher resolution methods of measurement must therefore be implemented.

This paper presents flow measurements that were conducted concurrently from two moored platforms in Strangford Narrows, an energetic tidal channel, separated by approximately 500m. Between the two locations a rocky outcrop exists in the channel and the characteristics of the flow vary significantly. Two collocated instruments were used to measure the flow characteristics at each location: a five beam ADCP (Nortek Signature 1000) and an ADV (Nortek Vector).

This paper compares and contrasts both the flow characteristics at each location and the turbulence measurements using the different instrumentation types. The combination of instrumentation enables improved characterisation of the flow.

***Keywords*— Tidal Stream; Acoustic Velocity Measurements; Field Data; Turbulence; Flow Characteristics**

I. Introduction

This paper investigates the temporal and spatial variability of tidally driven currents, including characterisation of the high frequency, 'turbulent' fluctuations. Inflow velocity fluctuations cause changes in the angle of attack on turbine blades . Thus, turbulence impacts a turbine's power performance,andload conditions and has been found to decrease turbine performance [CITATION Kri13 \l 2057] [CITATION Myc14 \l 2057], while increasing fluctuations in power output, [CITATION Milne2010 \l 2057]. However, increasing ambient turbulence has also been found to significantly improve wake recovery, thereby leading to overall increased power output when multiple devices interact [CITATION Mycek2014876 \l 2057]. Understanding of the velocity characteristics at deployment sites is therefore important for the tidal stream energy industry.

Tidal flow field data at high resolution and higher frequency to allow turbulence characterisation remains relatively scarce. Three or four beam ADCPs are often used for tidal flow resource assessment but are limited by their temporal and spatial resolution, due to factors such as beam spread and the assumption of flow homogeneity across their beams. Five beam ADCPs enable improved turbulence measurement as they allow an additional direct profile measurement of the velocity component in the direction of the device orientation and tend to enable higher frequency sampling. Acoustic Doppler Velocimeters (ADVs) enable high resolution turbulence measurements, but only at a single point close to the instrument.

This paper presents a current and turbulence measurement campaign conducted concurrently from two barge platforms moored in an energetic tidal channel known as Strangford Narrows, Northern Ireland. The barges were located approximately 500 m apart, on either side of a rocky outcrop, known as Walter's Rock. The characteristics of the flow vary significantly between the sites. Site 1 was the location of the barge used for the Queen's University Belfast (QUB) Tidal Turbine Testing 3 (TTT3) project, which tested various configurations of 1.5 m diameter rotors [CITATION Que17 \l 2057], on the same platform that was used for the previous TTT2 project [CITATION Jeffcoate20153 \l 2057]. The rotors were not deployed during the measurements presented in this study. Two collocated instruments were used to measure the flow characteristics at each location: a five beam ADCP (Nortek Signature 1000) and an ADV (Nortek Vector). A differential GPS unit was deployed on each barge to record the barge location, movement and heading. The measurements were conducted for three flood/ ebb cycles in August 2016.

This paper compares and contrasts both the flow characteristics at each location and the turbulence measurements using the different types of instrumentation. The paper focuses on variations in the mean velocity between

the two sites and investigates the turbulence by looking at the variation in TKE over the tidal cycle and in the frequency domain.

II. Measurement Site

The data presented was collected in Strangford Narrows, a channel that connects the Irish Sea to Strangford Lough (Figure 1). The currents in Strangford Narrows are dominated by astronomic tides of semidiurnal nature [CITATION jmse2010046 \l 2057]. The peak depth-averaged velocities in parts of the channel exceed 4 m/s, with peak velocities at the two specific locations in the range of 1.2-1.6 m/s. The location of the mooring arrangement for the barge at Site 1 was at 54°22.91 N 005°33.31 W. The location of the barge at Site 2 was 54°23.06 N 005°33.75 W. The nominal water depth at each site is approximately 10m and 20m respectively. The sites are well mixed and turbulence production due to buoyancy is negligible.

III. Experimental Setup

A. Instrumentation

The instrument setup at each location was replicated as closely as possible. One 1000 kHz Nortek Signature ADCP and one Nortek Vector ADV were deployed at each location. A Hemisphere DGPS unit was deployed on each barge; a Vector V103 GNSS Compass on Site 1 and a Crescent V100 on Site 2. A second ADCP was deployed at each location and configured to begin sampling 24 hours after the first, but the data from these ADCPs was not considered in this study.

The specifications and sampling configurations of the instruments can be seen in Tables 1 and 2. The position of the instruments on each platform depended on the mounting fixtures available. The instruments at Site 1 (Figure 2) were deployed in a stream-wise configuration, whereas the instruments at Site 2 were deployed across the flow (Figure 2). Tear drop profile foam fairing was attached to the Vector mounting poles to suppress vortex induced vibrations.

Table 1: ADV Sampling Configuration

	ADV 1 (Site 1)/ ADV 2 (Site 2)
Sampling Frequency (Hz)	32
Burst Interval (hours)	1
Samples per Burst	38400
Burst Duration (min)	20
Coordinate System	Beam
Sampling Volume (mm)	14.9
Nominal Velocity Range (m/s)	2.00
Depth (m)	1.75

Table 2: ADCP Sampling Configuration

	ADCP 1 (Site 1)	**ADCP 2 (Site 2)**
Acoustic Frequency (kHz)	1000	1000
Sampling Frequency (Hz)	8	8
Burst Interval	Continuous	Continuous
Coordinate System	Beam	Beam
No Beams	5	5
No Cells	25	47
Cell Size (m)	0.5	0.5
Blanking Distance (m)	0.25	0.25
Depth (m)	0.5	1

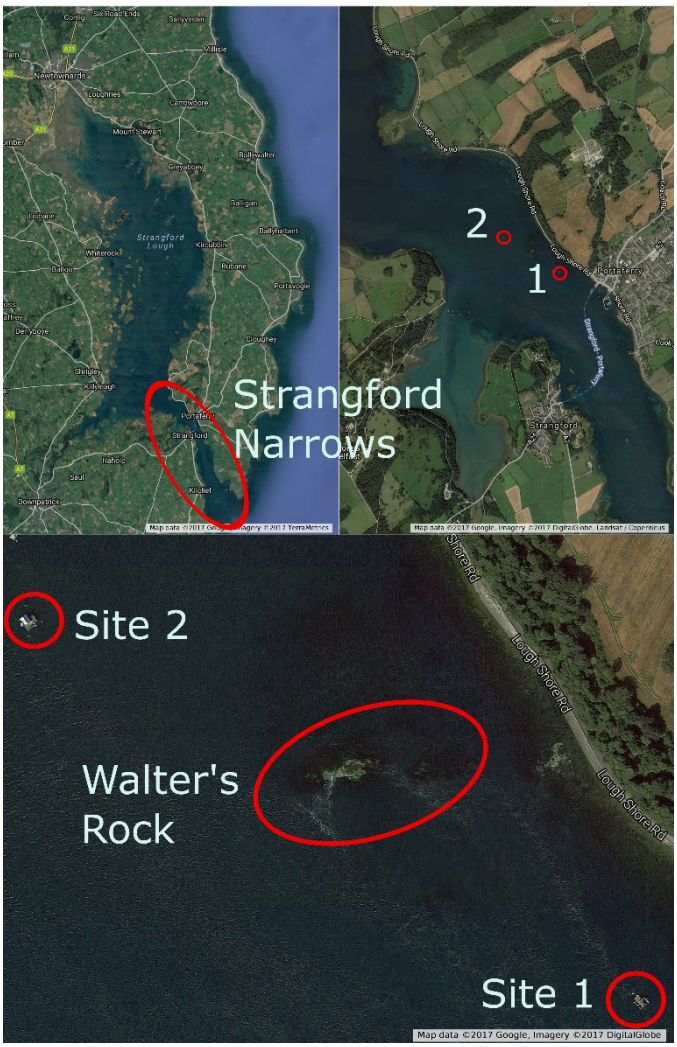

Figure 1: The location of the measurement sites in Strangford Narrows (Map data © 2017 Google, Imagery © 2017 DigitalGlobe/ TerraMetrics)

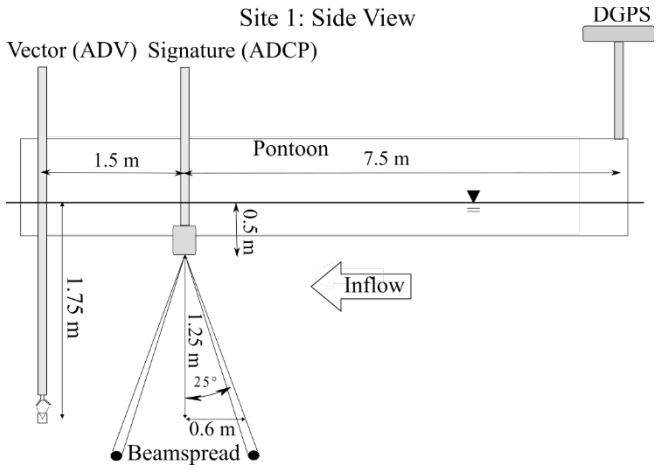

Figure 2: Schematic of the instruments at Site 1

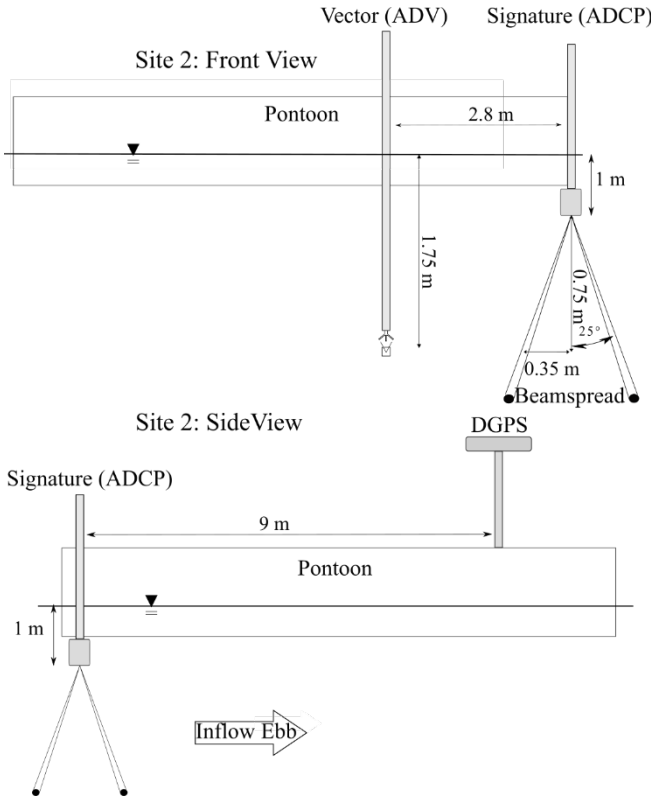

Figure 3: Schematic of the instruments at Site 2

The instruments began sampling at 16:00 British Summer Time on 19/08/2016 and recorded until memory or battery life limitations prevented further data collection (36 hours minimum). In this paper, only the first 24 hours of data are examined to avoid any possible effects of signal interference with the second ADCP.

B. Tide Conditions

Table 3 details the predicted tidal heights for Strangford for the deployment period [CITATION Tid16 \l 2057]. The measurements were conducted during a Spring tide, with the full moon on the 17th and 18th of August.

TABLE 3: PREDICTED TIDAL HEIGHTS

Date	Time	Tide Phase	Tide Height
19/08/2016	08:30	Low Tide	(0.33m)
	14:14	High Tide	(3.50m)
	20:36	Low Tide	(0.47m
20/08/2016	02:25	High Tide	(3.72m)
	09:09	Low Tide	(0.29m)
	14:52	High Tide	(3.53m)
	21:17	Low Tide	(0.45m)

C. Wind Conditions

The QUB Portaferry weather station was not functioning during the campaign, so the effects of wind on these measurements have not been investigated. However, an alternative source of local weather data will be located for further work.

D. Approximate Synchronisation

The laptop used for configuring the instruments for data collection was synchronised to an internet time server and the velocity instruments' Real Time Clocks were synchronised to the laptop time, using their deployment software. The DGPS satellite derived times agreed with the internet time at the beginning of the deployment. Clock drift over the relatively short deployment time has not been considered.

E. Barge Stability

The barge at Site 1 was connected to a single point mooring system, a chain attached to a mooring block on the seabed, and a two-point bridle system attached from the mooring buoy on the surface to the barge. The barge was therefore free to rotate and align to the incoming flow. The barge at Site 2 was connected to a four-point mooring system, so was not able to fully rotate and thus relatively more stable.

As both barges could move on their moorings (see Figures 4 and 5), the instruments were not continually measuring at the exact same position. Small, localised changes in flow conditions could therefore cause changes between samples. It is assumed that all samples are representative of the flow at a single location, but the DGPS coordinate data could be used to investigate this further. In terms of wave orbital velocities, Site 1 is more sheltered from wind generated waves than Site 2. However, Site 1 experiences the wash from the Strangford-Portaferry ferry approximately every half hour during the day.

The positions of each barge throughout the measurement period are shown in Figure 4. The DGPS output coordinates were converted from Latitude / Longitude to UTM (Zone 29N) using QGIS[CITATION QGI17 \l 2057], to give coordinates as a distance in meters from a reference. For ease of interpretation of the figure, the most westerly and southerly coordinate of each barge was used as the reference coordinate (point [0,0]). Figure 5 shows examples of the movement of each barge during two ten-minute time intervals; one around peak ebb and one around peak flood (as determined by the velocities at Site 1). The barge at Site 2 tends to drift more slowly and react less to changes in inflow conditions. RMS velocities for each ten-minute interval throughout the duration of the measurements, estimated from the change in position of the barge over time, are consistently lower at Site 2 than at Site 1. For example, for the ebb interval shown in Figure 5, the RMS velocity is 0.12 m/s at Site 1 and 0.06 m/s at Site 2, while during the flood it was 0.07 m/s and 0.04 m/s respectively.

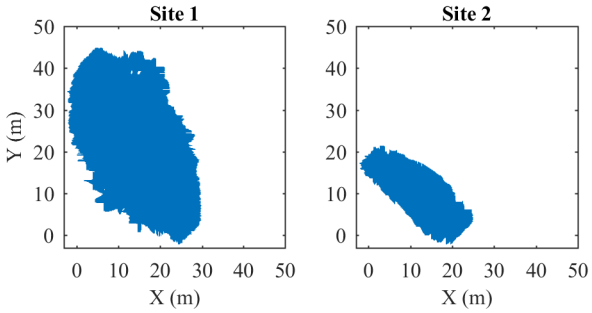

Figure 4: Position of each barge throughout the measurement campaign

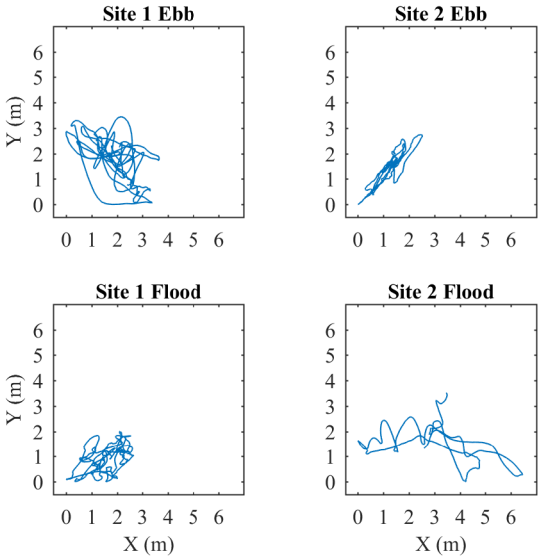

Figure 5: Position of each barge during two example ten-minute time intervals: one at peak ebb tide and one at peak flood tide

IV. Data Processing

The time series are separated into shorter intervals for analysis. Ten minutes is chosen as a suitable time window that captures the longest turbulence time scales but maintains stationarity, i.e. is not affected by the variation in the mean velocity due to the tidal forcing [CITATION Clark2015 \l 2057].

Assessment of the quality of Acoustic Doppler measurements is essential for ensuring reliable interpretation of velocity results. Errors caused by low signal strength, Doppler Noise, signal aliasing and other effects such as side-lobe interference can result in inaccuracies in the data. Such errors can render data inaccurate, causing increased data variance, bias of means and altered energy spectra results. Certain quality control procedures are therefore recommended by manufacturers and a number of organisations have developed open source quality control methodologies [CITATION Gunawan2011 \l 2057][CITATION Cote2011 \l 2057][CITATION Symonds2006 \l 2057]. The procedures implemented in this analysis are outlined in the following section.

A. Side- lobe Interference

To mitigate the effects of side-lobe interference, the bottom
10% of the Signatures' velocity profiles were removed [CITATION Siegel2010 \l 2057] [CITATION Elsaesser2016 \l 2057]. The depth at each location was estimated from the Signature data. As the instruments were surface mounted, the location of the seabed was approximated to the nearest cell location by locating the prominent rise in the return signal strength.

B. Amplitude/ Signal to Noise Ratio and Correlation

The validity of the results was also assessed according to the quality of the return signals. The consistency of returned signals within the sample volume in the sample period is measured by the percentage Correlation. Amplitude is a measure of the return signal strength, while Signal-to-Noise Ratio (SNR) indicates the strength of return signals compared to the instrument noise (Doppler Noise). As a quality control, unviable Vector data in this study are identified as having a Correlation of <70% or an SNR of <10dB. For the Signature data, a Correlation threshold of <50 % and an amplitude threshold of <30 counts was applied to identify invalid data [CITATION doi:10.1175/JTECH-D-16-0148.1 \l 2057].

Commonly, a SNR threshold of 15 dB is applied for Vector data [CITATION Ciochetto2007 \l 2057]. However, in this case the majority of data samples collected would have been rendered invalid if this cut-off were applied. The lower than expected SNR values are believed to be due to a low concentration of appropriate particulates in the water at the time of the measurements, due to seasonal variation.

C. Phase-Space Threshold Filtering

The true 3D Phase-Space Threshold (PST) filter, described in studies such as [CITATION Atcheson2012 \l 2057] [CITATION Mori2007122 \l 2057] is used to identify remaining spikes in the beam data after filtering data according to the quality criteria. This method evaluates the velocity signal, and its first and second time derivatives using a three-dimensional phase-space plot. Data points are assumed to be of good quality if they lie within the bounds of an ellipsoid, for which the three axes are calculated by multiplying the standard deviation of the velocity signal, its first derivative and second derivative respectively, by a universal threshold, λ.

$$\lambda = \sqrt{2 ln N} \qquad \text{Eq. 1 (a)-(d)}$$

where N is the number of data points.

Any points lying outside the ellipsoid are replaced. Commonly, this filtering is iteratively repeated until the number of outliers remains constant between iterations. In this case, to conserve variance, a maximum of three iterations were carried out.

D. Data Replacement

Throughout the processing outliers are replaced rather than removed. This is necessary to ensure data sets are continuous with respect to time, a requirement for frequency domain

spectral analysis. Invalid data points are replaced with the local mean, which has been found to conserve the statistics of the data well when only a small number of data points are replaced [CITATION Gunawan2011a \l 2057] [CITATION Durgesh201429 \l 2057]. A sample is deemed invalid if more than 10% of its data points require replacement.

E. Coordinate Transformation

Velocities measured in beam coordinates were transformed to earth coordinates using the instruments' transformation and heading and tilt matrices. Horizontal velocities were then rotated to the mean direction of the flow in each ten-minute window. This results in a stream-wise component in the direction of the mean flow, a perpendicular cross-stream component and a vertical component of velocity.

1) *Assessment of Tilt Measurements*

This deployment was conducted before the release of the Attitude Heading and Reference Sensor (AHRS) option for the Signature devices became available [CITATION Nor17 \l 2057]. Prior to this release, the Signature's tilt sensor, a solid-state accelerometer, enabled tilt to be calculated on the assumption that the device is stationary. Any deployment platform motion causes forces other than gravity to affect the accelerometer measurements and may thus affect the reliability of the tilt measurements. The pitch and roll from each instrument at each site are shown in Figure 6 below.

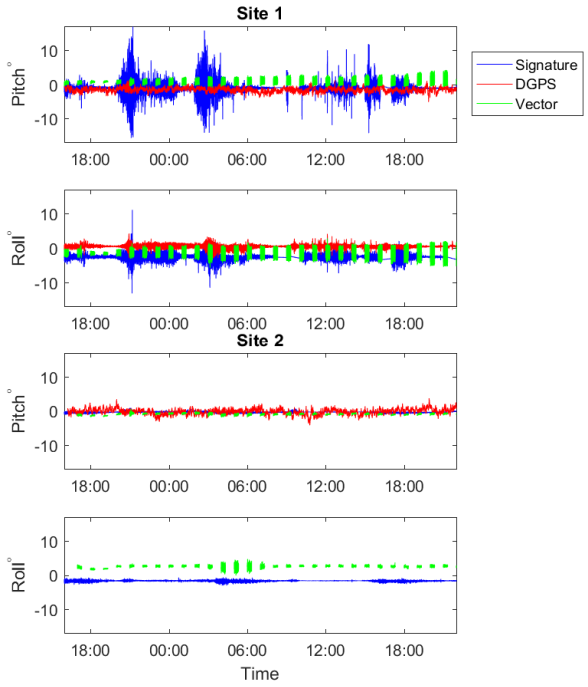

Figure 6: Pitch and roll from each instrument at each site

As a result of motion of the barge at Site 1, the tilt data derived from the Signature's accelerometer is somewhat unreliable. From prior knowledge of the barge system, the pitch data, in particular, is believed to be inaccurate, with values oscillating between +-17° at some points during the measurement period. Additionally, during quality control, concerns about the validity of the Vector's tilt measurements at Site 1 arose. Fluctuations observed in pitch and roll gradually increased throughout the measurement period. While vibration of the Vector mounting is possible, it is not believed to be the cause in this case, as the fluctuation does not ease around slack water. For this reason, the Site 1 Vector's tilt measurements are not deemed to be reliable. Therefore, the tilt data from the DGPS are applied to both the Signature and Vector data collected at Site 1. The mean values of pitch and roll for each instrument are deemed reliable and reflect the stable position of the instrument in its mounted position. The pitch and roll data from the DGPS are mapped to the Vector and Signature. The effects of this on the results shown in this paper are negligible.

As the barge at Site 2 is known to be more stable, it is believed that the Site 2 Signature's tilt data is more reliable. The instruments' tilt angles at Site 2 are small; less than 5° at all times and with maximum oscillations of +-2°.

V. Analysis

ADV data has been analysed using the authors' own code, except where otherwise stated. An open source code toolbox, '5Beam-Turbulence-Methods' [CITATION MGu17 \l 2057] was used as the basis for analysis of the Signature ADCP data, but has been adapted for the authors' requirements.

Mean flow velocities presented in this study are calculated from the Signature data. Velocities in earth coordinates are averaged over depth (all valid velocity cells) and time (ten minute windows) to calculate the mean flow speed and direction from North.

Turbulence is analysed using the Reynolds decomposition of a short term (stationary[CITATION Ben71 \l 2057]) time averaged velocity signal, into its mean ($\acute{u}$) and fluctuating ($u_i^{'}$) parts. The turbulent fluctuations are the deviations from the mean.

$$u_i = \acute{u} + u_i^{'} \qquad \text{Eq. 2}$$

The strength of the turbulence is assessed by calculating the TKE, a coordinate system invariant scalar.

$$TKE = \frac{1}{2}\left(u_1^{'2} + u_2^{'2} + u_3^{'3}\right) \qquad \text{Eq. 3}$$

A. Spectral Analysis

Spectral analysis of the turbulent fluctuations provides information about the distribution of turbulent fluctuations across the different timescales in the flow.

In this study, we invoke Taylor's Frozen Field hypothesis, which assumes that the turbulence is advected by the convective velocity, here taken to be the mean. Therefore, we can also investigate the spatial structure of the flow.

Kolmogorov hypothesises that, at sufficiently high Reynolds Numbers, turbulent flow will exhibit an inertial sub-

range. In this range the turbulence spectrum is proportional to $k^{-5/3}$, where k is the wavenumber. This is associated with an equilibrium cascade of energy from larger to smaller isotropic eddies, within a certain range of eddy scales [2]. The equation for the inertial subrange is:

$$S_1(k) = a_1 \langle \epsilon \rangle^{2/3} k^{-5/3} \qquad \text{Eq. 4}$$

where k is the wavenumber in rad/m, a_1 is the Kolmogorov Constant and ϵ is the dissipation. The integration of the spectrum over all frequencies is the total variance in the signal.

$$\sigma_1^2 = \int_0^\infty S_1(k)\, dk \qquad \text{Eq. 5}$$

Applying Taylor's Frozen Field hypothesis to Kolmogorov's theory, a slope proportional to $f^{-5/3}$ is expected in the inertial subrange, where f is frequency.

$$S_1(f) = a_1 \langle \epsilon \rangle^{2/3} \left(\frac{\acute{u}}{2\pi} \right)^{2/3} f^{-5/3} \qquad \text{Eq. 6}$$

where $\acute{u}$ is the convective (mean) velocity.

Spectra are calculated using Welch's overlapping segment method, using the 'pwelch' function in Matlab [CITATION 1720 \l 2057]. Each spectrum from each ten-minute interval is calculated by averaging the Fast Fourier Transform of eight overlapping 128 second data segments. Spectra are then grouped according to the phase of the tide during which they were measured (ebb/ flood), for comparison between sites and between instruments.

VI. Results

A. Depth and Time Averaged Speed at Each Site

The variation in depth and time averaged flow speed throughout the first 24 hours of data collection at each site is shown in Figure 7. Note that a gap in the figure shown for Site 1 exists between ~08:00 and 10:00, due to gaps in the data file. The cause of the gaps is unknown.

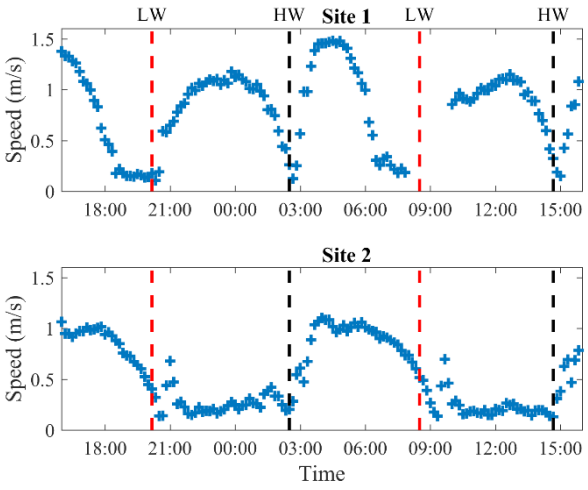

Figure 7: Mean depth and time averaged flow speed at each site. The approximate times of each low water (LW) and high water (HW) are indicated on the plot by the dashed vertical lines.

The velocities at Site 1 show a mixed semi-diurnal nature. Across the site, the flood tide is known to generally produce stronger currents than the ebb [CITATION jmse2010046 \l 2057]. However, at the locations investigated in this study, the peak ebb currents are stronger. The peak depth averaged speed at Site 1 reaches approximately 1.1 m/s on the flood tide. The current during the ebb tide accelerates and decelerates faster than during the flood tide, reaching higher peak velocities of approximately 1.5 m/s within a shorter time. During the last third of each ebb tide, the velocities drop off. This is due to the flow patterns in the region of Walter's Rock. When the channel between the two pinnacles of Walter's Rock dries out, Site 1 is subsequently in the lee of the outcrop. Additionally, as the tidal level drops, the passage between Walter's Rock and the shoreline changes, causing the direction of flow to deviate away from the location of Site 1.

At Site 2 peak depth averaged speeds of around 1 m/s are observed on the ebb tide, with a gradual increase and decrease within ~6-hour (half a tidal cycle). The mean speed during the flood tide remains around 0.2-0.3 m/s throughout, apart from a short, sharp increase in the speed near the start of the cycle. This peak in the velocity, observed at approximately 21:00 and 09:30, is known to consistently occur during all flood tides. The currents at Site 2 are weak during the flood tide because of the channel bathymetry and topography and the location in the lee of Walter's Rock. There is significant shear in the velocities across the channel in the region of the site and eddies, including a large back-eddy which generates in the bay in which the site is located, dominate the flow at the site.

F. Depth and Time Averaged Direction at Each Site

The variation in depth and time averaged flow direction throughout the first 24 hours of data collection at each site is shown in Figure 8.

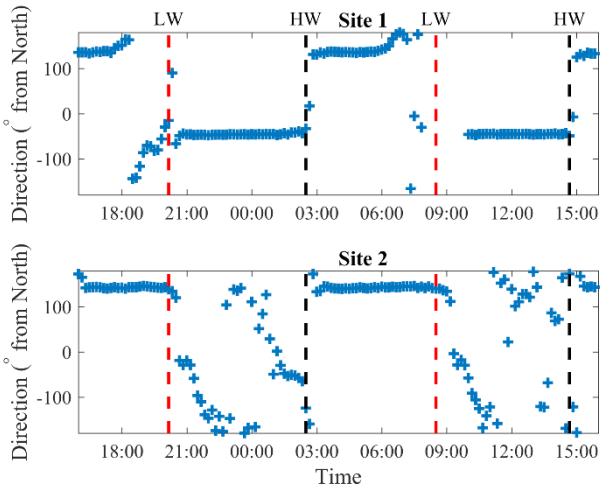

Figure 8: Mean depth and time averaged flow direction at each site

At Site 1 the flow direction reverses rapidly between the flood and ebb tide. The principal direction during the ebb tide is approximately 134° from North, while during the flood tide it is ~46°. The change in flow direction around Walter's Rock in the latter part of the ebb tides, as mentioned previously, can be seen.

At Site 2 the principal direction on the ebb tide remains relatively constant at ~142°. However, the mean flow direction varies throughout the flood tide. The variation of direction within each ten-minute interval is also large (data not shown). The variation in direction is caused by the eddies which dominate the flow, as discussed. The mean direction appears to exhibit a trend of a gradual clockwise rotation during the entire cycle. However, this is less apparent during the second half of the second flood tide measured.

G. TKE at Each Site

The variation in TKE over time at each site, as calculated from the ADV data, is shown in Figure 9. The TKE at Site 1 is generally stronger throughout the ebb tides, while significant peaks in the TKE at Site 2 are evident during the first flood tide measured. The TKE spectra at each site are presented in the following section and the differences between the sites are discussed.

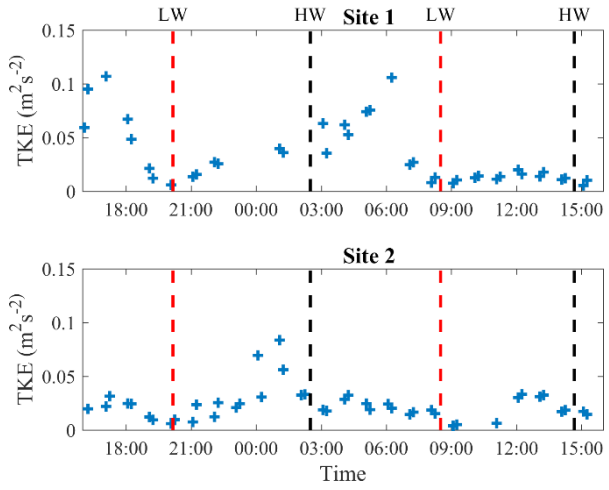

Figure 9: TKE variation with time at each site as calculated from ADV data

H. Turbulence Spectra at Each Site from ADV Data

Spectra of the turbulent fluctuations in the stream-wise (u_x), cross- stream (u_y), and vertical (u_z), velocity components are shown in the following sub-sections. The spectra illustrate the distribution of TKE with frequency. For comparison between sites, spectra are grouped according to the phase of the tide and averaged. Spectra from intervals which are valid for both ADVs (one at each site) according to the processing procedures are averaged, and the mean ebb and flood spectra are presented.

1) *Ebb:*

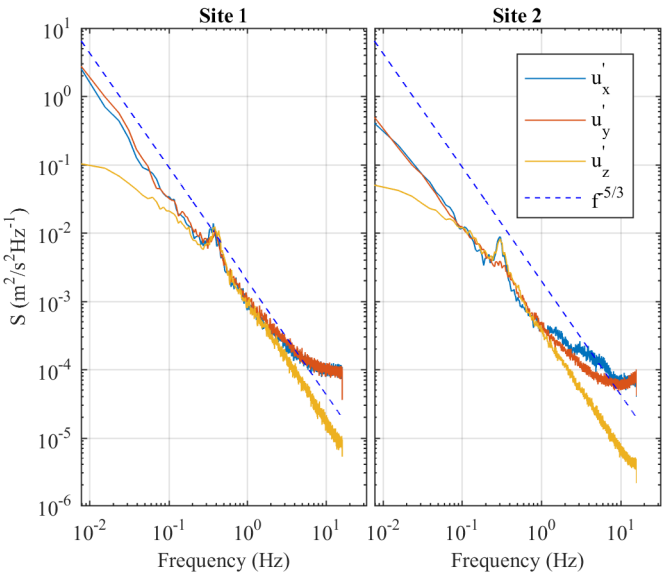

Figure 10: Ebb tide TKE spectra at each site from ADV data

The means of the calculated turbulence spectra during the ebb tides are shown in Figure 8. Three general regions of the turbulence spectra can be seen, as expected. In the low frequency range of the spectra (~below 0.2 Hz), the energy is greatest and there is significant anisotropy between the horizontal and vertical spectra at both sites. This region is due

to large scale, anisotropic eddies. In the mid-frequency range, the inertial sub-range can be observed where the spectra follow the $f^{-5/3}$ slope. The high frequency portions of the spectra are very low in energy and dominated by Doppler Noise, which has the properties of white noise. The stream-wise and cross-stream components, as expected, show a higher noise floor due to the geometry of the Vector sensor.

ADV measurements were taken at approximately 1.75 m below the water surface, which acts to suppress the vertical velocity fluctuations. The lower frequency limit of the inertial subrange is expected to be on the order of $f = \acute{u}/(2\pi L)$, where L is the distance to the surface.

Small bumps exist in the spectra in the region of 0.3-0.4 Hz. At Site 1 the bump is visible in all components while at Site 2 it is visible in the stream-wise and vertical components. This requires further investigation but is believed to be due to a combination of ferry wash/ barge movement at Site 1 and wind waves/ barge movement at Site 2.

Site 1 is more turbulent than Site 2 during the ebb tide. The amplitudes of TKE density spectra at Site 1 are greater than at Site 2. The difference at the low frequency, energy-containing scales is more significant than at the higher frequencies. The difference between the horizontal spectra is more significant than the difference between the vertical spectra. This is thought to be caused by the wake of Walter's Rock during the ebb tide. The eddies that shed from the outcrop have strong horizontal components.

2) Flood:

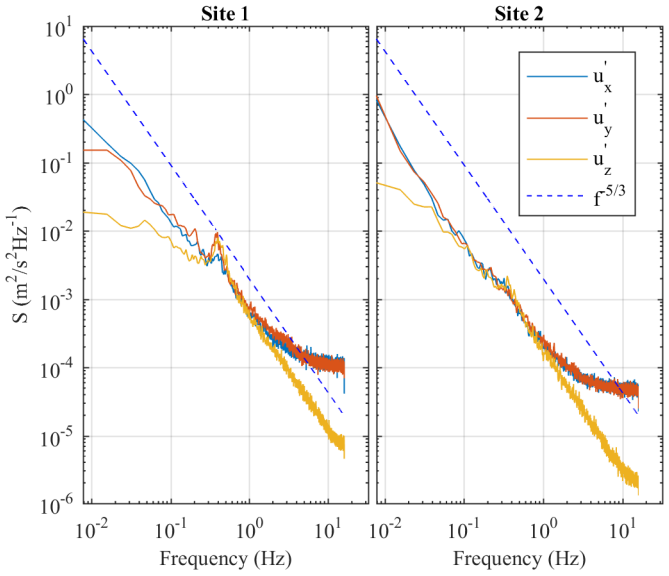

Figure 11: Flood tide TKE spectra at each site from ADV data

On the flood tide (unlike the ebb tide), there is more energy in the lower frequency scales at Site 2 than at Site 1. Again, this is believed to be in part due to Site 2 being downstream of Walter's Rock during this phase of the tide. It is known that the velocities at the site are dominated by large-scale eddies in this phase of the tide, causing significant low frequency fluctuations in the velocity.

I. Vertical Turbulence Spectra at Each Site from ADV and ADCP

When vertically orientated, the 5th beam of the Signature ADCP directly measures vertical velocity. The limiting scale for the smallest flow scale that can be reliably measured is then the cell size rather than the beam spread, as is the case for the velocity components resolved from angled beams.

A comparison of the vertical turbulence spectra generated from the ADCP vertical beam with those generated with the ADV is therefore interesting and is presented in the following sub-sections. At Site 1 the Vector measurement volume was located at the mid-point of Cell 2 of the Signature data, while at Site 2, it was aligned with Cell 1. The ADV spectra are compared to the ADCP spectra from the corresponding cell. Only intervals that are valid for both the ADV and the ADCP are included in the average. The number of intervals averaged is different for each site and between flood and ebb.

1) Ebb:

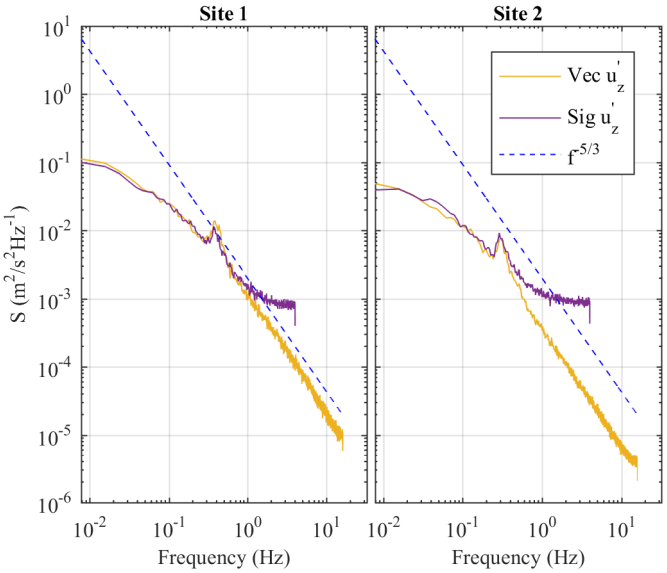

Figure 12: Ebb tide TKE vertical spectra at each Site: ADV and ADCP comparison

At both sites, the spectra according to the ADV and the ADCP vertical beam agree strongly at lower frequencies. The start of the inertial subrange is evident at both sites. The spectra of the two instruments at each site deviate from one another in the mid-high frequency range (~above 0.5 Hz) and the ADCP spectra flatten out at a higher level. This is as expected because the ADCP measurements have more inherent Doppler Noise. The deviation is also due to the fluctuations becoming smaller than the ADCP cell size of 0.5 m, and so they cannot be reliably measured.

3) Flood:

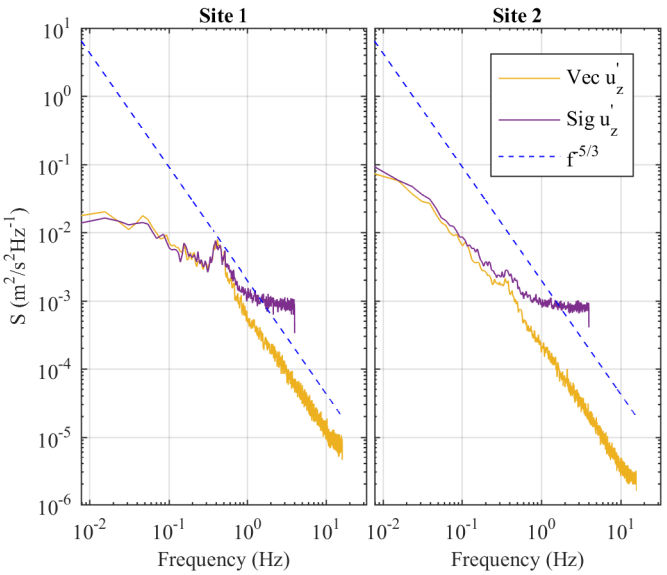

Figure 13: Flood tide TKE vertical spectra at each site: ADV and ADCP comparison

During the flood tide, the same trends are evident at higher frequencies due to the ADCP resolution and Doppler Noise. The ADCP spectrum at Site 2 is slightly offset from the ADV spectrum. The reason for this slight discrepancy is unknown but the difference is not significant.

The trends seen here agree with the results in [CITATION doi:10.1175/JTECH-D-16-0148.1 \l 2057], which compares spectra from a Nortek Signature ADCP and Nortek Vector ADV collected at different times in both Rich Passage and Admirality Inlet. This study concluded that the Signature successfully measured turbulence and found good agreement between the Signature and Vector vertical turbulence spectra.

VII. Conclusions

As a result of complex flow regimes through Strangford Narrows, flow characteristics vary significantly across the site. In this example, the mean flow characteristics at each location are different and change substantially between ebb and flood tides. The velocities at Site 1 are greater than at Site 2 throughout most of the tidal cycles observed. The exception is the latter part of the ebb tide, when the flow patterns in the region of Walter's Rock cause the velocity at Site 1 to drop off approximately 2 hours before low water. Site 2 experiences very little mean flow throughout the flood tide and eddies dominate the flow. The TKE strength varies between sites and between the ebb and flood tide. The relative position of Walter's Rock to the flow is believed to be a significant contributing factor to this, along with channel bathymetry and the shape of nearby headlands.

The results of this study show generally very strong agreement between the spectra generated from the Vector data and the Signatures' fifth beam. The low frequency, energy containing scales are captured accurately by the Signature and the beginning of the inertial subrange is observed. ADCPs remain the preferred method of inflow characterisation for tidal energy devices and as technology progresses, can provide more reliable information about flow structure.

VIII. Further Work

Further investigation is required into the differences observed between sites. The mechanisms which create the flow characteristics at each location will be investigated further by examining bathymetry data and comparing results to outputs from the Strangford Lough hydrodynamic model [CITATION jmse2010046 \l 2057].

Furthermore, investigation into the effects of deployment platform motion on the results is required. At Site 1 the DGPS tilt might be applied to the accelerometer data from the Nortek Signature, in order to remove the effects of gravity from the acceleration data.

Spectra of the accelerations can also be estimated and used to correct the velocity spectra shown. The DGPS coordinate data can also be further consulted to approximate velocity due to the horizontal movement of the barges.

Additional investigation into the TKE budget, the scales of turbulent motion and the anisotropy will be carried out. This will include examination of the coherency of the turbulence from along-beam ADCP velocities in this campaign and from two-point measurements conducted on the same platforms in succeeding measurement campaigns.

References

[1] K. Mikkelsen, “Effect of free stream turbulence on wind turbine performance,” Trondheim, 2013.

[2] P. Mycek, B. Gaurier, G. P. Grégory Germain and E. Rivoalen, “Experimental study of the turbulence intensity effects on marine current turbines behaviour. Part I: One single turbine,” *Renewable Energy,* vol. 66, pp. 729-746, June 2014.

[3] I. A. Milne, R. N. Sharma, R. G. J. Flay and S. Bickerton, “The Role of Onset Turbulence on Tidal Turbine Blade Loads,” in *17th Australasian Fluid Mechanics Conference*, 2010.

[4] P. Mycek, B. Gaurier, G. Germain, G. Pinon and E. Rivoalen, “Experimental study of the turbulence intensity effects on marine current turbines behaviour. Part II: Two interacting turbines,” *Renewable Energy,* vol. 68, pp. 876-892, 2014.

[5] Queen's Univeristy Belfast, “Tidal Turbine Testing,” 2017. [Online]. Available: https://www.qub.ac.uk/research-centres/cerc/ResearchGroups/MarineResearchGroup/OurResearch/TidalEnergy/TidalTurbineTesting/. [Accessed April 2017].

[6] P. Jeffcoate, R. Starzmann, B. Elsaesser, S. Scholl and S. Bischoff, “Field measurements of a full scale tidal turbine,” *International Journal of Marine Energy ,* vol. 12, pp. 3-20, 2015.

[7] L. Kregting and B. Elsäßer, “A Hydrodynamic Modelling Framework for Strangford Lough Part 1: Tidal Model,” *Journal of Marine Science and Engineering,* vol. 2, no. 1, pp. 46-65, 2014.

[8] 19 08 2016. [Online]. Available: https://www.tidetimes.org.uk/strangford-tide-times-20160819.

9] T. Clark, K. Black, J. Ibrahim, J. Hernon, R. White, N. Minns, T. Roc and S. Fisher, “Turbulence: Best practices for data processing, classification and characterisation of turbulent flows. A guide for the tidal power industry.,” 2015.

[10] B. Gunawan and V. S. Neary, “ORNL ADCP Post-Processing Guide and MATLAB Algorithms for MHK Site Flow and Turbulence Analysis,” 2011.

[11] J. M. Côté, F. S. Hotchkiss, M. Martini and C. R. Denham, “Acoustic Doppler Current Profiler (ADCP) Data Processing System Manual: U.S. Geological Survey Open File Report 00-458,” 2011.

[12] D. R. Symonds, “QA/QC Parameters for Acoustic Doppler Current Profilers,” 2006.

[13] E. Siegel, R. Riley and K. Grissom, “Performance of the Nortek Aquadopp Z-Cell Profiler on a NOAA Surface Buoy,” in *Proceedings of the IEEE/OES/CWTM Tenth Working Conference on Current Measurement Technology*, Monterey, 2010.

[14] B. Elsäßer, H. Torrens-Spence, P. Schmitt and L. Kregting, “Comparison of Four Acoustic Doppler Current Profilers in a High Flow Tidal Environment,” in *AWTEC 2016*, 2016.

[15] M. Guerra and J. Thomson, “TURBULENCE MEASUREMENTS FROM 5-BEAM ACOUSTIC DOPPLER CURRENT PROFILERS,” *Journal of Atmospheric and Oceanic Technology,* vol. 0, p. null, 2017.

[16] D. S. Ciochetto, *Data Quality of Nortek Vector ADV in the North East Channel of the Gulf of Maine May 2007,* 2007.

[17] M. Atcheson, “A large scale model experimental study of tidal turbines in steady flow,” 2012.

[18] N. Mori, T. Suzuki and S. Kakuno, “Noise of acoustic Doppler velocimeter data in bubbly flows,” *Journal of Engineering Mechanics,* vol. 133, no. 1, pp. 122-125, 2007.

[19] B. Gunawan, V. S. Neary and J. R. McNutt, “ORNL ADV Post-Processing Guide and MATLAB Algorithms for MHK Site Flow and Turbulence Analysis,” 2011.

[20] V. Durgesh, J. Thomson, M. Richmond and B. Polagye, “Noise correction of turbulent spectra obtained from acoustic doppler velocimeters,” *Flow Measurement and Instrumentation,* vol. 37, pp. 29-41, 2014.

[21] Nortek AS, “Signature1000 Release Notes,” 2017.

[22] M. G. Paris, “mguerrap/5Beam-Turbulence-Methods,” 2017.

[23] J. Bendat and A. Piersol, Random Data: Analysis and Measurement Procedures, New York: John Wiley and Sons Inc., 1971.

[24] MathWorks, “pwelch,” 2017. [Online]. Available: https://uk.mathworks.com/help/signal/ref/pwelch.html. [Accessed April 2017].

[25] Nortek AS, “Aquadopp Current Profiler User Guide,” 2008.

[26] Teledyne RD Instruments, “Teledyne RDI Library & Reference Center Glossary,” 2013. [Online]. Available: http://www.rdinstruments.com/glossary.aspx. [Accessed 04 December 2014].

[27] Teledyne RD Instruments, “WorkHorse Sentinel, Monitor, & Mariner Operation Manual,” 2014.

[28] Sontek, “SonTek/YSI ADP® Acoustic Doppler Profiler Technical Documentation,” 2000.

[29] Nortek AS, “Storm,” 2015. [Online]. Available: http://www.nortek-as.com/en/products/products-2/storm-surge. [Accessed March 2015].

[30] MathWorks, “nanmean,” 2013. [Online]. Available: http://uk.mathworks.com/help/releases/R2013a/stats/nanmean.html. [Accessed March 2015].

ACKNOWLEDGMENT

The authors would like to acknowledge the TTT3 project funders, Invest NI and CASE; the TTT3 project partners; Nortek for provision of a Signature 1000 ADCP; Minesto for

provision of instrumentation and facilities; and Cuan Marine Services for boating operations.